THE ASTROPHYSICAL JOURNAL, 267:665–681, 1983 April 15

FIRST OBSERVATIONS OF STELLAR CORONAL STRUCTURE: THE CORONAE OF AR LACERTAE

FREDERICK M. WALTER[1,2]
Joint Institute for Laboratory Astrophysics, University of Colorado and National Bureau of Standards
DAVID M. GIBSON[1]
Department of Physics, New Mexico Institute of Mining and Technology
AND
GIBOR S. BASRI[2]
Space Sciences Laboratory, University of California at Berkeley
Received 1982 August 2; accepted 1982 October 12

ABSTRACT

We have made *Einstein* IPC observations of the X-ray eclipses of the RS CVn binary AR Lacertae. These data, together with cotemporal *IUE* and radio observations, for the first time allow reasonable estimates of the structures of coronae of other solar-like stars. Under the assumption that the X-ray light curve is chiefly attributable to geometric effects, we find the following:

1. The X-ray luminosities of the G2 IV–V and the K0 IV components comprise about 40% and 60%, respectively, of the total.

2. Both components appear to have coronae with scale heights small ($\sim 0.02\ R_\star$) compared to the stellar radius. The inferred pressures and densities are similar to those found in small solar flares. Both coronae appear to require a large number (10^5–10^6) of magnetic loops to produce the observed emission.

3. An extended X-ray corona with a scale height of about 1 $R_\star$ appears to be associated with the K subgiant. Coupled with previously obtained radio data, this result suggests that some closed magnetic field structures may fill a volume comparable with the binary system itself.

4. The X-ray light curve requires that the corona of the larger K star be confined to equatorial latitudes.

5. Both the coronal and chromospheric surface fluxes appear to be inhomogeneous across the surfaces of the stars.

Subject headings: stars: coronae — stars: eclipsing binaries — stars: individual — stars: radio radiation — X-rays: binaries

I. INTRODUCTION

Prior to the advent of speckle interferometry, the only information astronomers had on the sizes, shapes, and surface features (e.g., spots) of other stars was gained through observations of eclipsing binary stars. Today, many of these same systems are again of interest because they exhibit detectable emission at X-ray or radio wavelengths. In a few cases the systems are sufficiently bright that, given new instrumentation such as the *Einstein Observatory*, the *IUE*, or the VLA, X-ray, UV, or radio light curves can be obtained which give structural information on the regions above the optical surfaces, the stellar coronae and chromospheres.

One system which is ideally suited for this type of study is the eclipsing RS CVn system AR Lacertae (Chambliss 1976). AR Lac is the brightest ($m_v = 6.2$) and nearest (40 pc) eclipsing RS CVn system. It is somewhat atypical of RS CVn systems (Hall 1976) in that both stars are above the main sequence, and both exhibit strong chromospheric activity (in most cases only one star, the more active component, is significantly evolved). The two components, G2 IV and K0 IV, have equal masses (1.35 $M_\odot$). The orbit is circular, with a period of $1^d.98319$ and a semimajor axis of 9.1 $R_\odot$. The orbital inclination is 87°: primary eclipse is total (G star eclipsed), and secondary eclipse is annular. The system is detached and is depicted (to scale) in Figure 9. The stellar radii and the orbital ephemeris are discussed in more detailed below.

The AR Lac system has long been known to exhibit characteristics of enhanced stellar activity, and each of

[1]Guest Observer with the *Einstein Observatory*.
[2]Guest Observer with the *International Ultraviolet Explorer* satellite.

the stars has been referred to as the more active. Historically, the first attribution of star spots on another star was given to the G star in AR Lac (Kron 1947) to explain irregularities seen during ingress into and egress from primary eclipse. Joy and Wilson (1949), Sanford (1951), and others have noted strong emission lines of Ca II attributable to both stars. Recent observations have shown AR Lac to be a radio emitter (Hjellming and Blankenship 1973) which occasionally exhibits large outbursts (Gibson and Hjellming 1974). AR Lac was first detected as an X-ray source with the *HEAO* 1 A-2 experiment (Walter *et al.* 1980) at a luminosity of $\sim 10^{31}$ ergs s^{-1}, comparable to the quiescent fluxes observed from all the other RS CVn systems (Walter and Bowyer 1981).

Because AR Lac is the brightest eclipsing RS CVn system, we decided to use it to investigate the structure of the coronae of RS CVn systems by obtaining *Einstein* X-ray observations over a complete orbital cycle and examining the X-ray eclipses or lack thereof. Swank and White (1980) had observed this system at both minima using the *Einstein* SSS and had failed to observe any evidence for eclipses. The observed flux level decreased by a factor of 2 between primary and secondary minima and was constant for ~ 0.1 cycles about each eclipse, which suggests that either the system was flaring during one observation, or that some other large scale intrinsic variation may have masked any geometric eclipses. An alternate explanation is that the coronae may be large compared to the stars. These observations were not supported by cotemporal observations at other frequencies, and Swank and White failed to obtain any data at quadrature ($\phi = 0.25$), when neither star is occulted.

Taken at face value, the Swank and White (1980) results imply that the geometrical extent of the X-ray coronae is large compared to either of the stars. This is consistent with N. Cohen's VLBI observations that the quiescent radio emission in the RS CVn system HR 1099 arises from a volume of radius between 1 and 10 times the size of the system (Feldman and Kwok 1979), and the lack of radio eclipses in AR Lac (Owen and Spangler 1977; Brown, Broderick, and Neff 1979), provided that the radio emission and the X-rays arise from the same population of electrons. In contrast, Walter *et al.* (1980) observed a rotational modulation of the X-rays in UX Ari, deriving a coronal scale height of $\lesssim 0.1\ R_\star$ in this system, and the Rosner, Tucker, and Vaiana (1978) loop scaling relations predict loop lengths of $\sim 0.1\ R_\star$ in these systems based upon the *HEAO* 1 observations. Because the electron densities derived from radio observations are two orders of magnitude lower than those implied by the X-ray emission, one might expect the radio corona to be more extended than the X-ray corona.

We proposed to reobserve this system through a complete orbital period with the *Einstein* Imaging Proportional Counter, which has greater sensitivity than the SSS, especially below 1.0 keV, where RS CVn systems are very bright. In principle, eclipse timing observations combined with depths of the eclipses can yield coronal radii, as well as information on the spatial distribution of the coronal gas. However, it is crucial that one be able to rule out the possibility that the observed variations are intrinsic rather than geometric and that the data can be interpreted in that context. The available information is greatly increased by observations at other wavelengths, which also help to guard against the possibility of misinterpreting variability due to large flares at about the time of an expected eclipse. Accordingly, we scheduled UV and radio observations cotemporally with the X-ray observations. Previous simultaneous observations of the similar system HR 1099 (cf. Weiler *et al.* 1978; White, Sanford, and Weiler 1978; Newell *et al.* 1979) have shown evidence for activity at all wavelengths during flares, including simultaneous X-ray and radio flaring. In particular, UV observations are sensitive to thermal activity in the chromospheres and transition regions, while the radio observations are sensitive to nonthermal flare phenomena in the outer coronae.

a) System Parameters

We have attempted to find and use the best available system parameters in this analysis. As is often the case, there is not unanimous agreement in the literature about the orbital parameters of AR Lacertae. For an eclipse timing investigation such as this, it is crucial to know absolute stellar radii and an exact ephemeris.

Recent ephemerides are summarized in Table 1. The apparent secular decrease in period ($\dot{P}/P \sim 4 \times 10^{-9}$) (Hall and Kreiner 1980; Kurutac *et al.* 1980), along with the possibility of discontinuous period changes (Hall, Richardson, and Chambliss 1976) complicate matters greatly in this case. The two quadratic ephemerides predict minima at the epoch of observation (JD 2,444,404) earlier than the linear ephemerides (although not significantly so in one case). The times of minimum light quoted by Chambliss (1976) and Srivastava (1980) (the most recent epoch) can be combined to yield an ephemeris similar to that of D. S. Hall (1981, private communication). In this paper we shall use Hall's linear ephemeris. The difference between that and Chambliss' ephemeris is important only for egress from primary minimum, and the impact of that uncertainty will be discussed later. We find that if we employ the quadratic ephemerides, the X-ray flux after primary minimum begins to increase only after some 15% of the G star should have reemerged from eclipse.

Because the system is eclipsing, stellar masses and radii can be determined. Popper and Ulrich (1977) quote radii of 1.8 and 3.1 $R_\odot$ for the G and K star, respectively; Chambliss (1976) quotes radii of 1.5 and

TABLE 1

AR LACERTAE EPHEMERIDES

Observation (s)	Primary Minimum (JD)	T_{min}(s UT 1980 June 13)
Hall	$2{,}439{,}376.4973 + 1^d.9831956E$	34,400
Chambliss 1976	$2{,}439{,}376.4955 + 1^d.9831987E$	34,923
Srivastava 1980	$2{,}442{,}716.1986 + 1^d.983198E$	34,569
Hall and Kreiner 1980	$2{,}426{,}624.3314 + 1^d.9832561E - 4.18\times10^{-9}E^2$	33,384
Kurutac *et al.* 1980	$2{,}441{,}593.7115 + 1^d.98319197E - 4.591\times10^{-9}E^2$	33,290
$(\text{Chambliss/Srivastava})_{av}$	$2{,}439{,}376.4955 + 1^d.9831966E$	34,467

2.8 $R_\odot$, respectively. Since the radii determined using the Barnes-Evans (1976) relationship, using colors and magnitudes quoted by Lacy (1979) agree with Chambliss' radii to within ~ 10%, assuming a distance of 40 pc (Chambliss 1976), we have adopted the latter radii. We have taken the K velocities from Batten, Fletcher, and Mann (1978).

The uncertainties in the absolute masses and radii will have lesser consequences in our analysis than the uncertainties arising from the choice of ephemeris. However, signal-to-noise ratio considerations limit us to using data binned in 500 s bins if we are to see flux variations at the 5% level. The heliocentric correction is of order 40 s and has been ignored.

b) Coronal Modeling Strategy

In any eclipse study with limited phase coverage, it is important not to overinterpret the data. In modeling the X-ray light curve, we have attempted to abide by this dictum. The models we have computed are of purely geometrical eclipses, with no intrinsic stellar variability permitted. The coronal flux distribution is assumed to be symmetric about the equator, and we have fixed the orbital inclination at 90°. We have used solar analogies and previous estimates of the coronal environment of RS CVn system as guides in modeling these data.

The corona is likely to be optically thin in X-rays (cf. Walter, Charles and Bowyer 1978) and hence will be limb brightened. Swank *et al.* (1981) have shown that the spectra of RS CVn systems can be represented as a two-component thermal plasma. Since the chromospheric and coronal activity in RS CVn systems is well represented by a scaled-up version of normal solar activity, the coronae of RS CVn systems are likely to be highly structured, with the emission confined to closed magnetic flux tubes (Vaiana and Rosner 1978; Walter *et al.* 1980). However, the observed emission measures require that there be a large number of individual loops, perhaps on order of 10^5–10^6 (Walter *et al.* 1980). In this case one is not likely to be able to separate the contributions from individual active regions. Thus, rather than modeling the corona as a set of discrete bright points, as is appropriate for the Sun, we model the corona of an RS CVn system as a shell or torus of uniform volume emissivity.

It is likely that the X-ray corona will be confined in latitude. In the Sun, the poles tend to be occupied by coronal holes, while the active regions are concentrated in bands at intermediate latitudes, which migrate toward lower latitudes as the solar cycle progresses. Evidence for such latitudinal migration is seen in RS CVn systems as well, in the phase drift of the photometric wave (Hall 1976). Additionally, it is unlikely that the corona will be longitudinally isotropic. The Sun shows preferred active longitudes, in which the active regions concentrate; the photometric wave in RS CVn systems presumably is evidence for the existence of preferred longitudes for the star spots on RS CVn systems. In our models the emission can be confined in a latitude band, and the emission flux can be modulated sinusoidally in longitude, with the wavelength of the modulation equal to the stellar circumference. We have also explored the possibility that large coronal holes might influence the light curve, perhaps by covering an entire hemisphere and making the X-ray corona highly asymmetric.

Even assuming that all the variation is geometric, the number of free parameters available in these simple models is enough that a multiplicity of models can describe the observed light curve. We shall use X-ray spectral information, as well as salient observations at other wavelengths to further constrain the possibilities and to produce a self-consistent, but not necessarily unique, description of the coronae of AR Lacertae.

II. OBSERVATIONS

The X-ray observations were made using the Imaging and Monitor Proportional Counters of the *Einstein Observatory* (Giacconi *et al.* 1979). The X-ray observations of AR Lac began at phase 0.023 (phase 0.0 is the midpoint of primary eclipse) on 1980 June 13 and ended 2 days later at phase 0.027. This gave a short "overlap" during primary eclipse. The total IPC exposure time was 29,414 s or 17% of an entire orbital period. The data were taken during 11 different spacecraft orbits, in the following order, centered on phases 0.03, 0.06, 0.19, 0.23, 0.26, 0.39, 0.42, 0.46, 0.49, 0.89, and 0.02. These

data include egress from primary eclipse, ingress into secondary eclipse, and both intervening quadratures. The average count rate at quadrature for the entire IPC energy band (~ 0.1–4 keV) within a radius of 25 pixels was 1.86 counts s^{-1}. The IPC gain remained fairly steady during these observations. The data were analyzed using the standard CFA *Einstein* analysis programs. The system was clearly detected in the MPC (~ 2–10 keV) as well, with an average count rate of 0.53 ± 0.02 counts s^{-1}. There is evidence for X-ray eclipses at both minima in both the IPC and MPC.

The radio observations were made at 10.48 GHz with the 46 m telescope of the Algonquin Radio Observatory. The observing procedure was identical to that used in previous observations of RS CVn systems and is given in detail by Feldman *et al.* (1978). There was no positive (3 σ) detection of AR Lac during any of the six radio flux measurements; the weighted mean observed flux over this orbital cycle was 3 ± 5 mJy. AR Lac was clearly not exceptionally radio-active during these observations.

The UV observations were obtained with the *IUE* on 1980 June 13 UT, as detailed in Table 2 (see Boggess *et al.* 1978 for a description of the *IUE*). The first low-resolution short wavelength (SWP-LO) spectrum was obtained mainly during primary minimum; the first low-resolution long wavelength (LWR-LO) spectrum was also obtained during totality. The final high-resolution long wavelength (LWR-HI) spectrum, although somewhat underexposed, was obtained at quadrature and clearly shows the Mg II emission in each component. This exposure (LWR 8029) and the preceding SWP-LO exposure (SWP 9275) were shorter than desired due to high radiation levels during a US 2 shift. Additionally, prior to SWP 9275 the camera was prepared with a SPREP procedure followed by an XSPREP, rather than in the standard opposite order. We have examined these exposures carefully and find them quite usable and apparently trustworthy, although somewhat noisier than the earlier observations.

The X-ray count rates are plotted in Figure 1, along with the times of the UV and radio observations. The IPC data are plotted in 500 s bins, the MPC data are summed in larger bins to improve the signal-to-noise ratio. Times of the contacts are indicated for each eclipse (first and fourth contacts are the points of external tangency at phases 0.92 and 0.08; second and third contacts represent the points of internal tangency at phases 0.98 and 0.02).

Before describing those variations in the light curve that are probably due to geometric effects, we note that there is considerable short-time-scale variability outside eclipse in this system, far more than any we have seen in other similar systems, such as UX Ari or HR 1099. Most notable is the rapid increase in the count rate beginning at phase 0.25. We comment on this aspect of AR Lac's behavior first because, although there is no evidence for unusual cotemporal activity at radio wavelengths, where we do have overlap there does seem to be evidence for intrinsic X-ray variability at the 10% level, and this variability may mask geometric variations or lead to misinterpretations. With this cautionary note in mind we will try to remain rather conservative in our interpretation of this X-ray light curve.

The observations obtained at phases 0.2 and 0.9 should be uncomplicated by stellar occulations and should represent the maximum flux from the system in the absence of any net longitudinal asymmetry. The two observations have identical mean count rates (1.86 counts s^{-1}), a fact which supports this contention. We use this value as the mean stellar X-ray flux and will refer all eclipse observations to this value.

The two observations of primary minimum prior to third contact, separated by one orbital period, also yield identical X-ray fluxes of 1.24 counts s^{-1}, which appears to be a quiescent flux associated entirely with the K star. The repeatability of the flux levels at the primary minima and the quadratures, together with the lack of detectable radio emission limits gives us confidence that we are dealing with a quiescent nonflaring corona.

a) Gross Aspects of the X-Ray Light Curve

To provide an overview of the X-ray light curve, we have broken the light curve up into four discrete segments, representing primary eclipse prior to third

TABLE 2

UV OBSERVATIONS

Image	Dispersion	Phases	Exposure (m)	Note
SWP 9273	low	0.968–0.999	90.	
LWR 8016 ...	low	0.002–0.003	2.5	During totality
LWR 8017 ...	high	0.046–0.060	40.	
SWP 9275	low	0.061–0.080	55.	Nonstandard camera preparation
LWR 8018 ...	low	0.082–0.083	2.5	
LWR 8029 ...	high	0.253–0.259	17.	Slightly underexposed

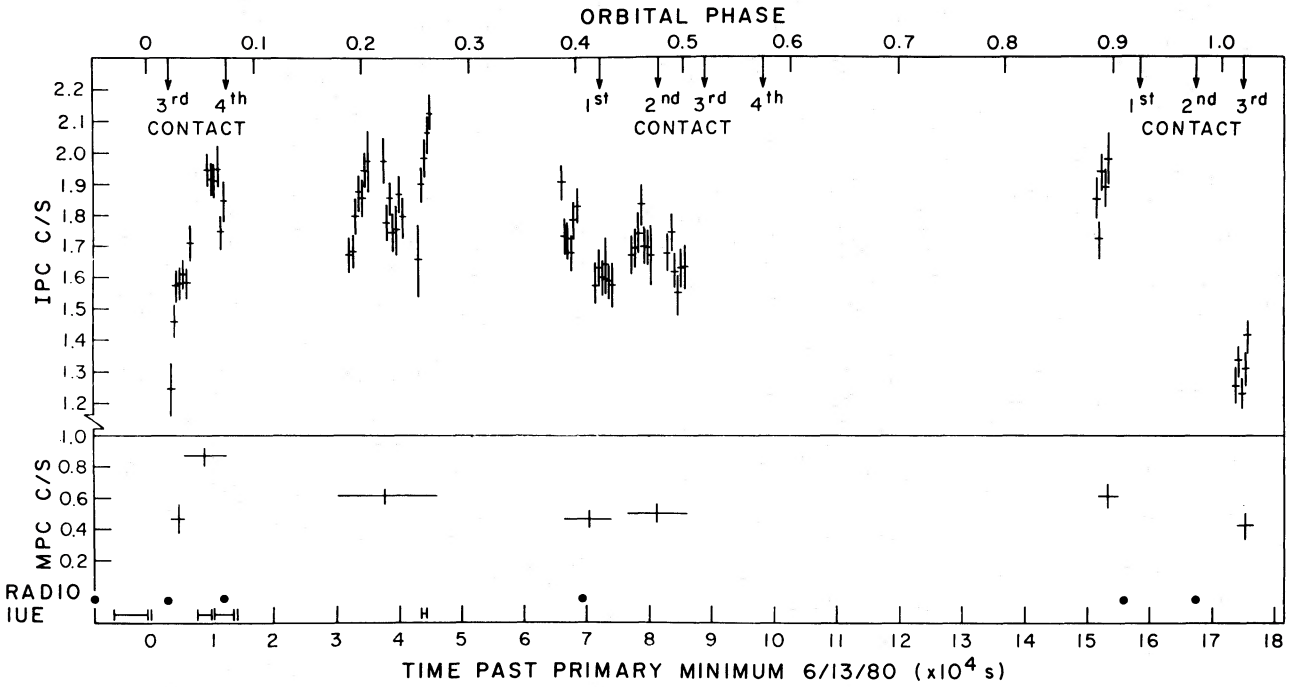

FIG. 1.—The X-ray light curve of AR Lacertae. IPC data is summed in 500 s bins; the MPC data is summed each sequence (2000–12,000 s), except for the first sequence which is in two segments. The abscissae show time past phase 0 (mid-primary eclipse) and orbital phase. Times of contacts are indicated. The data show a deep eclipse at primary minimum, followed by rapid egress, and a broad shallow secondary minimum. We also show the times at which the radio and IUE observations were made.

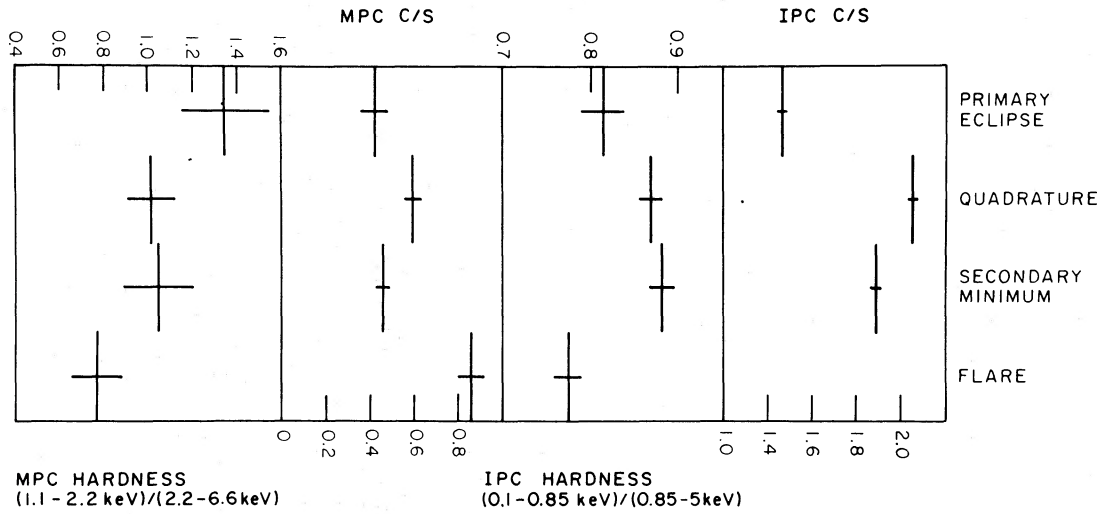

FIG. 2.—The gross characteristics of the light curve. We have binned the X-ray data taken at primary minimum (totality), quadrature, secondary minimum, and during the possible flare during egress from primary minimum. Eclipses are clearly seen during the minima. The hardness ratio is significantly lower (hotter spectrum) during the flare.

contact, secondary eclipse, quadrature, and a possible X-ray flare during egress from primary eclipse. These count rates and hardness ratios are plotted in Figure 2.

The highest count rate observed in the IPC was observed at quadrature, with the count rates at secondary and primary minima depressed by 9% and 32%, respectively. Since primary eclipse is total, and the count rate prior to third contact is constant, we feel confident in attributing 1.24 counts s^{-1} of X-ray flux to the K star plus any greatly extended emission either in the system

or associated with the G star (the observed X-ray background is 0.03 counts s^{-1}). Thus, 30% of the total projected X-ray flux in AR Lac must arise in a volume comparable in size to the G star, and the K star contributes at most 68% of the projected flux.

At secondary eclipse the IPC count rate is depressed by an average of 9%, or by at least 14% relative to the K star contribution. This depressed count rate is observed for 2×10^4 s prior to mid-eclipse; during that time a minimum of 54% of the available flux from the K star is obscured. It seems that the corona of the K star cannot be longitudinally isotropic.

Relative to the count rate at quadrature, the two minima in the MPC behave similarly. The count rate at primary minimum is depressed by 30% as was the IPC count rate; that at secondary minimum is depressed 23%. The eclipse depths at primary minimum as measured by both the IPC and MPC are identical. The different depths of secondary minimum in the two instruments may be interpreted as due to two coronal components. The hotter component, preferentially detected by the MPC, must then be highly concentrated on the leading edge of the K star since a 23% eclipse for the 2×10^4 s observation eclipses some 90% of the total flux.

Hardness ratios show no significant change at either of the two minima, as compared with quadrature, in either instrument (although in the IPC primary minimum is hotter at the 2 σ level). Within the errors, the spectra of the two stars are similar. The IPC spectra will be discussed later.

Note in Figure 2 that the highest count rate in the MPC, and the hardest spectra in both the MPC and IPC, occur during egress from primary minimum. (Because of the rapid variability of the IPC count rate, shown in Fig. 3, we have not computed a mean count rate during this interval.) The MPC count rate does not show a smooth increase but rather appears to double in less than 10^3 s (see Fig. 3) and then remains constant for nearly 4000 s. We may have observed a small flare, a bright flaring region on the leading hemisphere of the G star being uncovered during the emergence from eclipse or a flaring region on the K star rotating into view. These possibilities will be explored later. Nonetheless, this behavior clearly complicates analysis of the X-ray light curve during egress.

b) Spectra of the Individual Components

In principle it is possible to separate the spectra of the two components, if primary eclipse in X-rays is indeed total. To do so, we must assume that no significant X-ray flux arises in any very extended (1–2 $R_\star$) component of the G star corona, or in any unbound component. The latter is unlikely since the corona must be confined by magnetic flux tubes (cf. Walter *et al.* 1980). The former is difficult to rule out, but the rapid start of egress from primary eclipse, together with the lack of

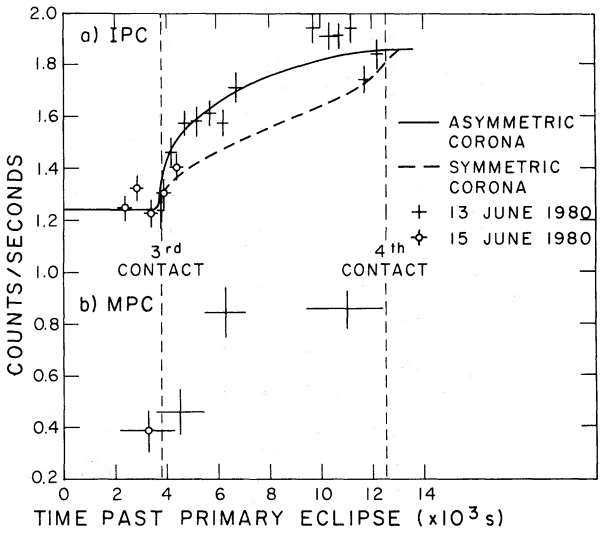

FIG. 3.—Egress from primary minimum in the IPC and MPC. Note the repeatability of the start of egress after one orbital cycle. The solid curve represents a longitudinally asymmetric, limb brightened corona, and represents egress fairly well. The dashed line shows the expected light curve from a longitudinally symmetric limb brightened corona. The steep increase by a factor of 2 in the MPC count rate may be attributable to the uncovering of a flaring region during egress.

any observed flux diminution at $\phi = 0.9$, imply that the G star corona is far less extended than the K star corona. Therefore, we assume that the IPC spectrum obtained during primary minimum prior to third contact is the spectrum of the K star alone. By subtracting the K star spectrum from that obtained during quadrature, one can determine the spectrum of the G star. The two spectra differ at the 88% confidence level, with the G star as a whole appearing cooler than the K star. (This shows as well in the 2 σ difference in hardness ratio mentioned in the previous section.) While this result is not significant, it is consistent with the spectral results derived from SSS observations (Swank *et al.* 1981; Agrawal, Riegler, and White 1981) that in the RS CVn systems with late-type (K) active components, including AR Lac, the hot coronal component contributes some 50% of the flux, while in those with earlier spectral types (α Aur, σ CrB) the cool component is much more dominant. Perhaps the hot ($T \gtrsim 2\times10^7$ K) spectral component is found primarily in the later type convective stars.

The K star spectrum cannot be adequately represented by a one-temperature Raymond-Smith (1980) thermal spectrum but is well represented by a 1 keV thermal bremsstrahlung spectrum, as Walter, Charles, and Bowyer (1978) found for UX Ari. Swank *et al.* (1981) have shown that RS CVn X-ray spectra are well represented by the sum of a cool ($T \sim 7\times10^6$ K) and a hot ($T \gtrsim 2\times10^7$ K) spectral component with

comparable fluxes. We have synthesized two-component thermal spectra in order to attempt to fit the K star spectrum, using cool components with temperatures (kT) between 0.6 and 1.0 keV, and hot components with $2.5 \leqslant kT \leqslant 5.0$. The IPC is remarkably insensitive to the temperatures of the individual components but is very sensitive to the relative fraction of each component. At 90% confidence, $0.42 \leqslant H \leqslant 0.54$, where H is the fraction of the observed flux in the hot component.

III. MODELING OF THE ECLIPSES

a) Primary Minimum in X-Rays

An expanded view of the egress from primary minimum is shown in Figure 3. The two independent sets of data overlap; both show egress beginning within a few hundred seconds of third contact. Egress is rapid and is complicated by the flare observed in the MPC which began ~ 1800 s after third contact. We assume that until that time we are observing reemergence of the quiescent corona of the G star. We have attempted to reproduce the gross features of the egress using a limb brightened coronal model as described earlier.

The rapid egress beginning at and not significantly before third contact shows that the height of the corona must be small. A vertical extent of as much as 5% of the stellar radius appears to be ruled out (although one could reproduce the time of egress by restricting a larger corona to high latitudes). The curves in Figure 3 represent models with slab heights of 0.02 $R_\star (2 \times 10^9$ cm). The dashed curve, which fails to reproduce the rapid egress, is for a longitudinally symmetric corona; the solid curve is a model with the flux modulated sinusoidally in longitude, with maximum emission on the leading hemisphere. This provides a good description of egress. These models have the emission arising between 10° and 40° latitude. There are no strong constraints on the latitudinal extent of the emission, except that it cannot all occur at or near the poles.

We feel that the departure from symmetry cannot be attributed to the flare. The increase in count rate just after the third contact, but prior to the onset of the flare in the MPC as well as the egress on June 15, are more rapid than predicted by the symmetric model. Mg II observations in the UV (see below) can be interpreted in context of an asymetric chromosphere as well. While the flare certainly complicates matters, the corona and chromosphere of the G star cannot be longitudinally uniform.

The measurement of the vertical extent of the corona depends crucially upon choice of ephemeris. Although Hall's ephemeris appears to be the best choice, there is some uncertainty. Chambliss's ephemeris predicts third contact later by some 530 s, which would increase the coronal radius to 0.11 $R_\star$. In any event, the corona is small compared to the stellar radius.

The high count rate prior to fourth contact, which exceeds the observed quadrature count rate, may be attributable to the flare observed in the MPC. If so, it is puzzling that no significant enhancement is observed in the IPC between 5600 and 6900 s past mid-eclipse, when the flare was first observed in the MPC. We shall discuss the flare more thoroughly below.

We conclude that it is likely that the corona of the G star is small, with a vertical extent of ~ 0.02 $R_\star$, and that the leading hemisphere of the star is brighter than the trailing hemisphere. The reproducibility of the X-ray light curve near third contact argues strongly that the gross features of this eclipse are, in fact, geometrical in nature. The smooth egress, along with the lack of activity in the radio, reinforces this argument. The X-ray flare commences well past third contact and fails to seriously weaken any of our conclusions.

b) Secondary Minimum in X-Rays

In Figure 4 it is apparent that there is no sharp secondary eclipse, although there is a marked depression in the count rate below the value observed at quadrature. The first data were obtained some 6000 s prior to first contact, and even at this phase the count rate is significantly reduced, implying a very extended corona about the K star. Minimum flux occurs near first contact, with a 22% reduction in the K star X-ray flux measured with the IPC, as might be expected for a very extended limb brightened corona. As explained earlier, the corona must be asymmetric, since a symmetric eclipse would occult some 10% more flux than can be attributed to the K star.

It is not possible to fit these data self-consistently with a single simple coronal model for the K star. In light of the spectral data, which require two distinct coronal components of equal observed flux, we have attempted instead to describe these data as an eclipse of a corona with two spatial components. The extended component presumably corresponds to the hotter spectral component, while the cooler spectral component is presumably located closer to the photosphere. With the constraints that half the flux is in the hot extended component, the data prior to first contact require that this component be asymmetric, with a brighter leading hemisphere. It must lie between 0.5 and 1.0 stellar radii above the surface and must be highly confined in latitude in order to obtain as deep an eclipse as is observed. We emphasize that observed eclipse depth cannot be obtained unless the corona is anisotropic in longitude.

This extended component, fitted by eye to the count rates prior to first contact, also describes the upward trend observed after first contact until about 7000 s prior to mid-eclipse. The inner component, which is required to explain the low count rates at mid-eclipse, cannot extend significantly above the photosphere; in fact, a limb brightened corona extending 2×10^9 cm

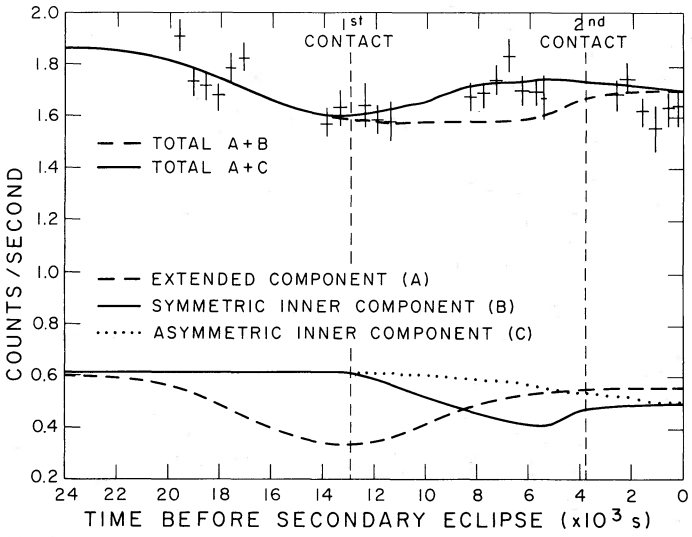

FIG. 4.—Ingress to secondary minimum seen by the IPC. The eclipse is broad, with the lowest count rate near the time of first contact. We need two coronal components to model this eclipse. The dashed line in the lower panel is the light curve of the extended component; the solid and dotted curves represent the contribution to the count rate from symmetric and asymmetric limb brightened coronae. The summed light curves (including the flux from the G star) are plotted through the data. The extended component plus an asymmetric inner component follows the trends in the data best, but, as discussed in the text, the phase coverage is not sufficient to tightly constrain the morphology of the inner corona.

above the photosphere produces a flat light curve between first contact and ~ 5000 s prior to mid-eclipse. We have constrained the latitude limits of the inner components to be the same as those required for the extended component and require that half the observed flux arise in this component. Models incorporating symmetric and asymmetric limb brightened coronae are plotted in Figure 4. The asymmetric curve fits the data far better than any of the other simple models but requires the enhanced hemisphere to be diametrically opposite the enhancement in the extended component. Because of the paucity of data on the inner component, we consider the geometry of this component essentially unknown, except that it is small in vertical extent.

Contour plots of the projected X-ray surface brightness measured at Earth as seen at phase 0.0 for the G star and 0.5 for the K star are shown in Figure 5. The extreme confinement in latitude of the extended component of the K star is striking. All models are symmetric about the equator.

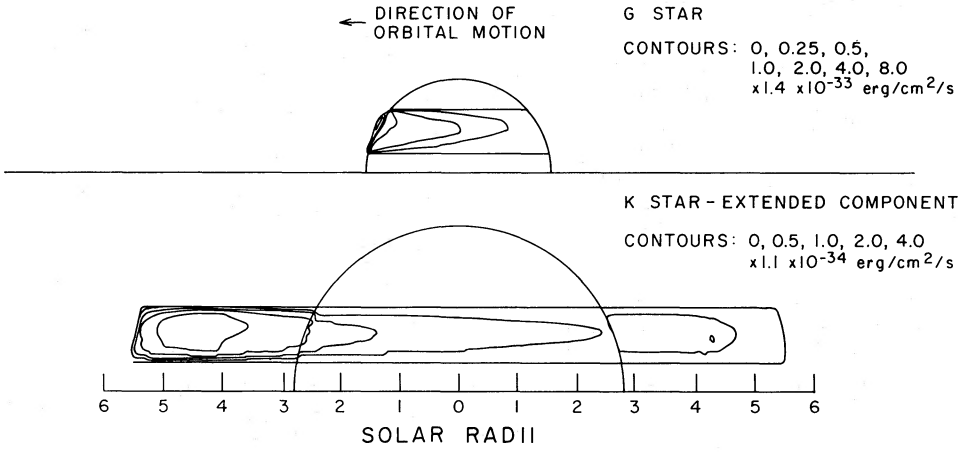

FIG. 5.—Contour plots of the projected X-ray flux from the two well-determined coronal components, as seen from the direction of the substellar point on the other star. The direction of orbital motion is to the left in both cases. The extended component of the K star is highly confined in latitude. The contours are in units of observed projected surface flux.

c) *Primary Eclipse in the Far-Ultraviolet*

We display the two far UV spectra we obtained with *IUE* at primary minimum and around fourth contact in Figure 6. The lower spectrum is that of the K star alone; the upper spectrum is the sum of both stars (with two-thirds of the K star hemisphere the same as in the first spectrum). During totality the K star exhibits a rather normal RS CVn chromospheric and transition region spectrum, with the usual range of emission lines from the chromosphere (e.g., O I λ1302 and Si II λ1816) to the transition region (e.g., N V λ1240 and C IV λ1549). The line strengths in the latter exposure are about 50% greater across the board. Within the errors, the two stars have similar spectra. These lines and their measured fluxes from both spectra are given in Table 3. The composite spectrum suffers from the observational difficulties mentioned earlier which render it somewhat noisier than desired. The nonstandard camera preparation led to some streaking in the background which appears as the large negative intensity features in the spectrum. Because of the nonstandard preparation we cannot fully trust the photometric reduction and can only appeal to the apparent consistency of the zero level and some of the stronger lines in the two spectra. The hotter photospheric continuum of the G star is readily apparent at the longer wavelengths.

d) *Primary Eclipse in* Mg II *h and k*

Four long wavelength UV observations of the system were obtained during and after the first primary eclipse (see Table 2). The two high dispersion observations are displayed in Figure 7. The first of these was taken when half the G star had appeared from behind the K star (velocity separation ~ 80 km s^{-1}), and the second was obtained almost exactly at first quadrature (velocity separation ~ 230 km s^{-1}). At first glance the profiles look rather as one would expect; there is a blueward component which remains more or less constant between the two observations, while the redward component is slightly smaller during the eclipse and more than doubles by quadrature. The surprising aspect of this behavior is that for a primary eclipse it is the *uneclipsed* star which yields the redward component! Thus, the two stellar components are behaving in rather opposite fashion from what one would expect if each star were uniformly covered with chromospheric emission.

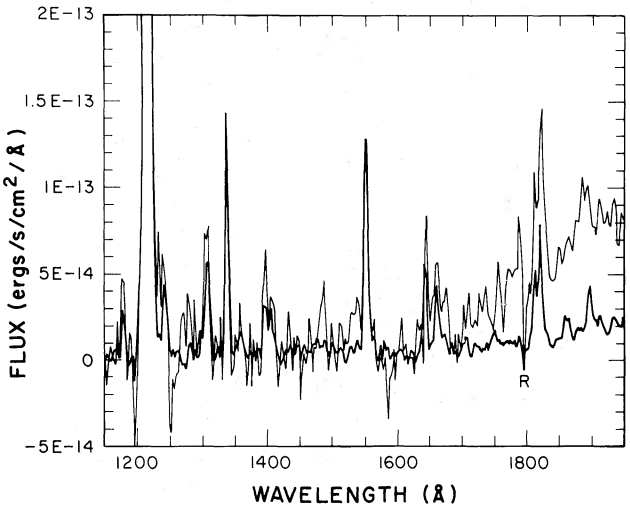

FIG. 6.—Far-ultraviolet spectra obtained at the first primary eclipse and its egress. The thick line shows the K star flux; the thin line shows the increased flux due to the G star having almost fully emerged. Negative intensities are due largely to the nonstandard camera preparation. The usual complement of chromospheric and transition region lines are visible.

The only reasonable explanation for these observations is that by the time half the G star is uncovered we are already seeing most of the activity which is present on the hemisphere visible at quadrature, while the K star was presenting a rather inactive face at phase 0.05 compared to what is visible at quadrature. Because we know the system parameters fairly well, we can use these observations to make quantitative statements about the distribution of chromospheric activity by deconvolving the profiles of the individual stars from their composites. A very basic procedure was found to be quite adequate for our purposes: we reflected the outer wings of the two components in the quadrature observation about their peaks to get canonical *h* and *k* line profiles for each star. We then normalized the line intensities so they matched the observation when added together. Using the separate profiles, we can compare the partial eclipse and quadrature fluxes for each star. We find the expected velocity separations for the two observations. For the *k* line we observe an increase of one-third in the G star flux and a factor of 2.6 for the K star between the two LWR-HI observations. The increases in the *h* line are approximately 85% of these. Midway into the first observation, the G star passed through the 48% exposed point (note that the time resolution of most of the *IUE* observations is much worse than the X-ray observations). Because the flux from the G star only increased one-third from there to quadrature, we see that the inner (facing the K star) leading quadrant had ~ 3 times as much plage area as the outer leading quadrant.

Despite the fact that during egress the K star presented 6 times the surface area of the G star, its total Mg II flux is actually slightly less than that from the G star. There must have been very little activity present on the hemisphere of the K star facing away from the G star. By first quadrature, the flux from the K star had increased by a factor of 2.6, leading to a surface flux two-thirds that of the G star. To get a better idea of the extent in longitude of the quiescent region on the K star,

TABLE 3

ULTRAVIOLET LINE FLUXES

LINE	SWP 9273 (primarily K star) f[a]	SWP 9273 (primarily K star) F[b]	SWP 9275 f[a]	SWP 9275 F[b,c]
C III λ1175	0.2	0.08	0.3	0.05
N V λ1240	0.31	0.12	0.34	0.54
O I λ1302	6.2	2.4	8.0	1.3
C II λ1335	6.3	2.4	8.5	1.4
O I λ1356	1.5	0.57	1.8	0.29
Si IV λ1392	2.5	0.96	5.0	0.80
Si IV λ1403	2.6	0.94	3.4	0.54
C IV λ1549	10.	3.8	12.0	1.9
He II λ1640	4.2	1.6	5.6	0.89
C I λ1657	4.1	1.6	7.1	1.1
O III + Al II λ1666	1.5	0.57	4.7	0.75
Si II λ1808	3.2	1.2	3.2	0.51
S I + S II λ1820	6.4	2.4	11.0	1.8
Si III λ1892	3.0	1.1	2.7	0.43
C III λ1909	1.1	0.42	1.1	0.18

	LWR 8017 f[a]		LWR 8017 F[b]		LWR 8029 f[a]		LWR 8029 F[b]	
	G	K	G	K	G	K	G	K
Mg II *h*	2.85	2.62	3.64	1.00	3.17	6.59	4.05	2.52
Mg II *k*	2.56	2.47	3.27	0.944	2.70	5.60	3.45	2.14

[a]Observed fluxes in units of 10^{-12} ergs cm^{-2} s^{-1}.
[b]Surface fluxes in units of 10^{6} ergs cm^{-2} s^{-1}.
[c]Surface fluxes assumed equal on both stars.

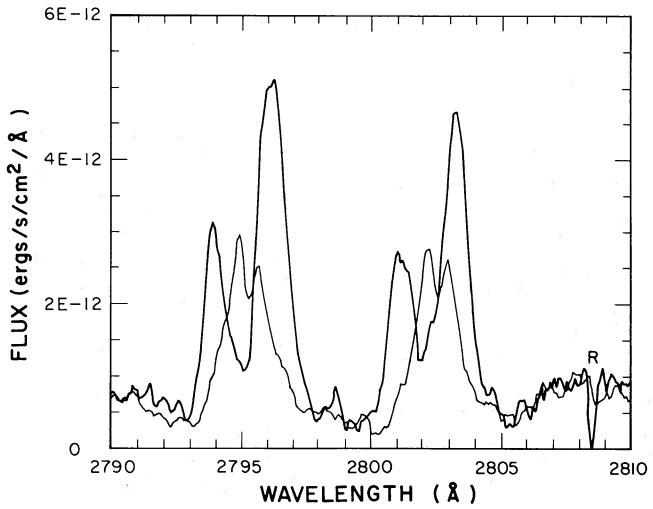

FIG. 7.—High-resolution observations of the Mg II resonance lines during egress from primary minimum (*thin lines*) and at quadrature (*thick lines*). Approximately half of the G star is visible at this stage of egress. Note that although the G star is the one eclipsed, it produces the approximately constant blueward component, while the K star shows a dramatic change (having remained unocculted). The flux ratios of K to G star is 2:1 at quadrature, indicating the G star actually has stronger surface flux here.

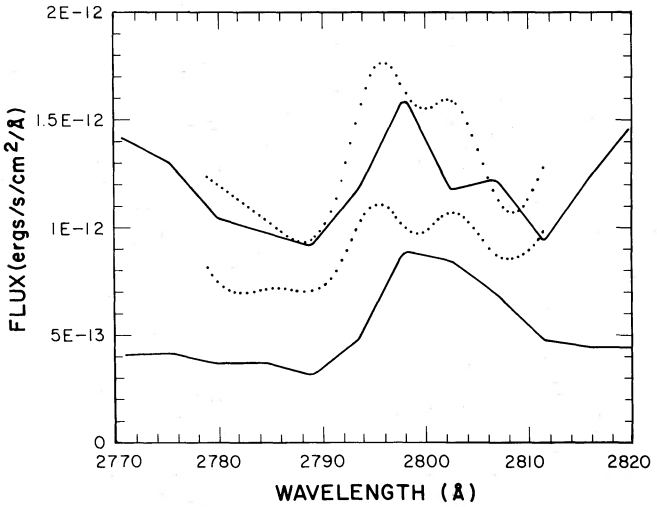

FIG. 8.—The appearance of Mg II at four phases at low resolution. The second and fourth (*dotted*) spectra are high-resolution observations which we have degraded by a 8 Å FWHM Gaussian profile. We have used the photometric calibration supplied for the low-resolution observations, and 3.39×10^{-13} ergs s^{-1} cm^{-2} $Å^{-1}$ fn^{-1} to convert the high-dispersion observations to absolute flux. From bottom to top the phases are 0.002, 0.053, 0.082, and 0.256. The observations show a steady increase in flux with phase, except that there is little difference between the last two (when essentially both stars were visible, though rotated somewhat between the two exposures). Note there are only ~ 8 pixels in the emission features for the low-dispersion observations (so noise is important), while hundreds of pixels are degraded in the high-dispersion profiles.

we make use of Mg II fluxes obtained from the other two (low-resolution) exposures. These are shown in Figure 8, along with the high-resolution observations degraded appropriately (we merged two echelle orders and used an 8 Å FWHM Gaussian instrumental profile). The low-resolution profiles are much more subject to noise because they are only covered by a few pixels, rather than the hundreds present in the high-resolution observations. Nonetheless we see that both the absolute continuum and line flux levels in the latter two exposures and all the line shapes are fairly consistent. The total flux measurements for the four profiles with the continuum subtracted are (chronologically) 6.7, 3.6, 6.7, and 8.4 ($\times10^{-12}$ ergs cm^{-2} s^{-1} $Å^{-1}$). Taken at face value, these imply that between $-70°$ and 110° longitude (0° is defined as the substellar point, and longitude increases in the same way as phase in Fig. 9) on the K star there was much less chromospheric activity than immediately preceding or following. The evidence of activity in the first (LWR 8016) exposure is bolstered by the strong fluxes observed just before in SWP 9273. The argument that soon after the first high-resolution observation (LWR 8017) the plage area visible had increased is strengthened by not only the flux level but also the shape of the next low-resolution observation (LWR 8018), which looks very much like that at quadrature. This implies that within a 10° slice on the inner trailing quadrant, some major plage regions had made their appearance. It also suggests that much of the activity visible at quadrature had already appeared be-

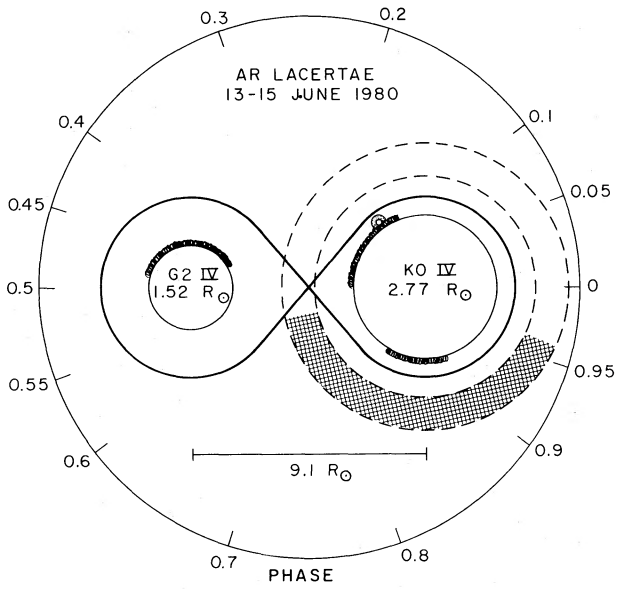

FIG. 9.—A scale drawing of the AR Lacertae system. The line of sight at a given phase is found by lining up the phase indicated on the outer circle with the center of mass. The solid line is the Roche surface; the dashed lines surrounding the K star indicate the inner and outer radii (1.5 and 2.0 R_k) of the extended component of the K star corona. We have indicated crudely the location and extent of the observed chromospheres and coronae. Note that the extended component of the K star coronae exceeds the Roche radius. The flaring loop on the K star occurred at the longitude indicated by the loop, which is not drawn to scale ($R_{\rm loop} \lesssim 0.05$ $R_{\rm K}$).

tween phases 0.06 and 0.08. A schematic representation of the state of AR Lac is given in Figure 9.

The general picture which is emerging from all of this is that homogeneous chromospheric models may be unacceptable for very active stars because such geometrical confinement implies much higher surface fluxes in the plage areas. This should be viewed only as suggestive; a far more comprehensive set of observations is required to clarify this point.

e) *The Flare*

The simplest explanation for the observed doubling of the MPC count rate is that it is due to a flare on a visible face of one of the stars. This hypothesis cannot be ruled out, but it is unlikely because no evidence for flaring was observed at any other wavelength at that time. Solar flares tend to exhibit enhancements at all frequencies simultaneously. Possible flare-related enhancements in the IPC and at Mg II occur later by ~ 1 and 2 hours, respectively. No radio flaring was observed, but the bracketing radio observations were taken prior to the MPC flux increase and subsequent to fourth contact by which time the radio flare, if any, may have decayed away.

A second possibility, suggested by the rapid rise time of the MPC X-ray flux, is that a flaring region on the G star was uncovered during egress. If so, the rise time puts a limit on the linear size in the orbital plane of the flaring region of $< 2\times10^{10}$ cm. If the region lies near the equator, then it is some 50° from the substellar point and in any event was visible to the detectors through the first quadrature observation, but the enhanced count rates were no longer evident by that time.

No significant radio emission was observed just prior to fourth contact (the flux was 11 ± 5 mJy at 10.48 GHz). If the linear size of the flaring region is $\sim 2\times10^{10}$ cm, one can estimate, using $V = L^3$, the particle density in the flaring region to be of order 10^{11} cm^{-3}. The plasma frequency at this density is ~ 18 GHz, so the lack of radio detection of this compact active region may not be surprising.

This possibility is supported by the observation that the leading limb of the G star is bright in both X-rays and UV; it is quite possible that some of this concentration of activity is due to the flaring. Simon, Linsky, and Schiffer (1980) observed a large flare in UX Arietis in the UV. They found that the transition region ($T \sim 10^5$ K) line fluxes increased relative to the chromospheric ($T \sim 10^4$ K) line fluxes by about a factor of 2. If, as they assume, the soft X-ray fluxes are enhanced by the same factor as the transition region flux, then the factor of $\lesssim 2$ enhancement observed in X-rays during this flare would correspond to an expected Mg II flux enhancement of $\sim 50\%$. Subtracting the expected flare enhancement, the chromospheric surface flux on the inner leading quadrant of the G star is still twice that in the outer leading quadrant. However, the lack of any enhancement in the soft X-rays until much later is inconsistent with this picture.

A more plausible assertion is that the flaring region was located over the inner trailing quadrant of the K star and rotated into view. The hard X-ray enhancement began near phase 0.033. The soft X-ray enhancement began by phase 0.05, and the Mg II flux from the K star bean increasing by phase 0.082. This sequence suggests a scenario whereby the hard X-rays come from the top of the flaring loop; the soft X-rays arise lower down; and the chromospheric plage lies near the footprints of the loop. Taking the Mg II flux from the K star between phases 0.046 and 0.060 as unenhanced, since it is similar to that during primary minimum, we can set a geometrical limit on height of the flaring loop, and we find that the hard X-ray emission comes from an altitude of between 0.01 and 0.05 $R_\star$ ($2\times10^9 < R < 9\times10^9$ cm) above the limb. The soft X-ray emitting region then lies $\sim 0.01\ R_\star$ below the hard X-ray emitting region. In this case most of the factor of 3 enhancement in the Mg II emission on the K star is flare related. The decay time for the flare in X-rays is shorter than the chromospheric decay by at least 10^4 s. The implied flare volume is smaller than that discussed above, leading to a higher plasma frequency and a good likelihood that no radio detection should have been expected. The flare footprints lie near stellar longitude 300°.

Kane *et al.* (1979) spatially resolved a solar flare, finding that the hard, impulsive component arose between 2.5×10^9 and 5×10^9 cm above the loop footprints, and that the soft X-ray flare arose entirely below 2.5×10^9 cm altitude. Our hard component is not a solar-like impulsive X-ray burst, since it was observed for some 3 hours, but it is remarkable that the altitudes we derive for the flare on AR Lac are so similar to those observed on the Sun. We suspect similar mechanisms are indeed at work.

IV. DISCUSSION

a) *On the Credibility of the Interpretation*

These data are unique, yet there are also serious deficiencies in phase coverage. Neither eclipse was fully covered, yet we find we require nonuniform chromospheric surface fluxes to explain the X-ray light curves and UV spectra. Cognizant of these limitations, we have restricted ourselves to certain simple, plausible models. All our interpretations must be viewed in this light.

The gross light curve does show both minima, and the depth of primary minimum and the unocculted (quadrature) count rates are repeatable over an orbital cycle. Excluding the flare during egress, there is no evidence for flaring in either the radio or the UV data, although

the X-ray flux varies at the 10% level on timescales of $\sim 10^3$ s. The amplitudes of both eclipses are greater than this, and secondary minimum occurs over a time of $\sim 2\times10^4$ s. We conclude that the coronae of AR Lac are indeed eclipsed. The problem arises in interpreting the details of the light curve.

Primary minimum appears to be flat-bottomed, consistent with a total eclipse of a small corona on the G star. Egress begins rapidly, which is consistent with the hypothesis of a thin, limb brightened corona, but more rapidly than is possible for a symmetric corona if flux is conserved. The complication with egress is that the MPC count rate, beginning just past third contact is higher than the quadrature count rate. The IPC count rate, prior to fourth contact, also exceeds the quadrature count rate. Furthermore, the spectra in both instruments are significantly harder than at other times during this observation. This strongly suggests that we observed a flaring region rotating into view. The radio observations bracket, but do not overlap, the times at which the X-ray count rate was enhanced. Nonetheless, the hypothesis is consistent with all the data.

It is hard to see how a long depression in the X-ray count rate can occur, except through a geometric occultation (other than by rotational modulation of a nonuniform surface), since stellar activity is generally associated with increased stellar flux in chromospheric and coronal lines (although the optical flux from flare stars sometimes decreases prior to large flares; Giampapa *et al.* 1982). The coincidence of the X-ray flux decrease and the phase of secondary eclipse makes it likely that secondary minimum is indeed a geometric eclipse. The depth of the eclipse at first contact constrains the extended coronal component, provided one associates it with the hot spectral component, as seems reasonable. Because the data stop at mid-eclipse, it is not possible to constrain the inner component well. There is, of course, a best fit in terms of our simple models, but it may not be physically realistic. Yet it is interesting that the inner trailing quadrant of the K star does seem to be bright in the UV and is consistent with the asymmetric inner coronal model. We caution that this (and any) light curve can be reproduced by judicious placement of bright patches on the stellar surfaces. Observations past mid-eclipse clearly would have clarified the ambiguities in the interpretation of these data.

We conclude that these observations do unmask several salient features of the spatial distribution of the coronal and chromospheric activity in the AR Lacertae system:

1. The G star corona is small, limb brightened, and has a brighter leading than trailing hemisphere.

2. The K star has a coronal component which contributes half the projected X-ray flux from the K star, is confined in latitude, is brighter in the leading hemisphere, extends approximately one stellar radius above the photosphere, and is probably the hotter spectral component.

3. There is another X-ray emitting component closer to the photosphere of the K star, which also contributes half the projected K star X-ray flux at phase 0.5.

4. Even during "quiescence," the X-ray flux varies at the 10% level, either due to intrinsic variability (flaring?) or rotational covering and uncovering of active regions.

5. There is strong evidence in our Mg II observations for patchy chromospheric emission, with quadrant-to-quadrant surface flux variations of a factor of 3, and possibly more extreme variations on smaller scales.

b) Inferred Physical Parameters

Using the observed coronal parameters and the coronal volumes from the models, one can infer coronal pressures and densities. Furthermore, one can estimate coronal loop parameters using the formalism of Rosner, Tucker, and Vaiana (1978). These quantities are given in Table 4.

The emission measures derived are temperature dependent, but we feel that the assumed temperature distribution is reasonable, given all the data. The temperatures are similar to those measured by Swank and White (1980). The coronal volume is derived directly from the constraints on the models. With these constraints the electron densities and pressures follow directly. However, these are mean values, averaged over the entire coronal volume. To mimic the observed asymmetry, the model employs a sinusoidally varying volume emissivity; thus, the electron density on the bright side of the star will be larger than the mean density by $\sim (2)^{1/2}$, and the electron density will approach zero on the other hemisphere. Pressures will vary similarly. These coronal pressures and densities are *not* model dependent. However, we have assumed a unit filling factor; hence, the true pressures and densities are likely to be larger than stated in Table 4. Loop lengths and the number of loops are computed following Walter *et al.* (1980). In estimating the number of loops N, we set $\alpha = 0.1$ ($2\pi\alpha^2 L^3$ is the volume of the loop, where L is the loop length).

We have attempted to estimate the chromospheric and transition region pressure using far UV line ratios (cf. Doschek *et al.* 1978*b*). Following the discussion of Simon and Linsky (1980), we have measured the C III λ1909/Si IV λ1403 ratio, assuming that 80% of the λ1403 blend is Si IV. Using the normalized curves in Doschek *et al.* (1978*a*), we derive an electron density of $\sim 10^{11}$ cm^{-3}, and a pressure $P = 2n_e kT = 1.7$ dyn cm^{-2} for the K star, for a temperature $T = 6\times10^4$ K. Assuming the flux from the K star is constant between the two SWP observations, we can estimate the G star fluxes. We find that I(C III/Si IV) < 0.22, or $N_e \gtrsim 2\times10^{11}$

TABLE 4

AR LACERTAE CORONAL PARAMETERS

Component	G	$K_{extended}$	K_{inner}	Flaring Sun[a]
Observations:				
Count rate (counts s^{-1})	0.62	0.60	0.61	...
Emission measure (N^2V)	5×10^{53}	2×10^{53}	5×10^{53}	10^{54}
T_x(K) (assumed)	8×10^6	3×10^7	8×10^6	10^7
I (C III λ1909/Si IV λ1403)	0 ± 0.22	...	0.55 ± 0.15	...
Model parameters:				
Coronal radius ($R_\star$)	1.0–1.02	1.5–2.0	1.0–1.01	...
Latitude bounds (degrees)	10–40	10–30	10–30	...
Coronal volume (cm^3)	1.5×10^{32}	2.4×10^{34}	3.0×10^{32}	4×10^{32}
Derived quantities (corona):				
$\bar{N}_e$ (cm^{-3})	5.9×10^{10}	2.9×10^9	4.1×10^{10}	5×10^{10}
$\bar{P}$ (dyn cm^{-2})	96	24	67	140
Pressure scale height ($H/R_\star$)	0.22	2.72	0.73	...
Derived quantities (transition region):				
$\bar{N}_e$ (cm^{-3})	$>2\times10^{11}$	...	10^{11}	...
$\bar{P}$ (dyn cm^{-2})	>3	...	1.7	...
Loop parameters[b]:				
L (cm)	1.9×10^9	(4.1×10^{11})	2.8×10^9	7×10^8
$L/R_\star$	0.02	(2.1)	0.01	0.01
Number of loops	10^6	(10)	8×10^5	7×10^5

[a]Solar surface half covered with small (Class C) flares, from Vaiana and Rosner 1978.

[b]Temperature of extended components of K star corona exceeds upper temperature for which the Rosner *et al.* formalism was derived.

cm^{-3} and $p \gtrsim 3$ dyn cm^{-3}. This is considerably less than the pressures we derive for the coronae and may indicate that bright, hot coronal loops are not isobaric (assuming that the observed transition region flux arises in the same loops). On the other hand, perhaps the extremely bright coronae of this and other active stars and their chromospheres arise in two populations of loops.

The fourth column in Table 4 shows typical values for an extremely active, flaring Sun, as taken from Vaiana and Rosner (1978). The similarities in N_e, P, L, and N to those values computed for the G star corona, show that our models may be reasonable in light of the assumption that RS CVn activity is a manifestation of extremely enhanced solar activity (Hall 1972; Walter *et al.* 1980).

The derived values for the inner component of the K star are similar to those of the G star. Although the numbers quoted are for the asymmetric model, a symmetric inner corona yields nearly identical results. The values derived for the extended component of the K star are also given, although the assumed temperature of this component exceeds that for which the Rosner *et al.* formalism was derived; thus, the derived loop parameters may not be physically meaningful. Here the derived pressure, densities, and loop lengths are much larger, as might be expected, and the number of loops is small. One interesting point to note is that in each case, the loop length predicted by the Rosner *et al.* formalism agrees well with the observed limits on the coronal radius. Since the loop lengths are far shorter than the pressure scale heights, the assumption of constant pressures loops appears valid. The confinement of the loops below the pressure scale height, but at radii in excess of the Roche surface in the case of the extended component of the K star, is strong evidence for magnetic confinement of the coronal gas, as seen on the Sun and generally assumed for all late-type stars.

The small number of loops estimated for the extended component of the K star emission may explain the fact that the hot component of RS CVn systems varies more than does the cool component (Swank *et al.* 1981). If the intrinsic coronal variability, exclusive of flaring, is due to the net variability of the individual loops or active regions, then there should be a general anticorrelation between the number of loops and the fractional variation. Structures of the size and temperature observed in the extended corona of the K star have no solar analog.

These large loops may be instrumental in generating the large flares observed at radio (Feldman *et al.* 1978) and UV (Simon, Linsky, and Schiffer 1980) wavelengths in RS CVn systems. Simon, Linsky, and Schiffer (1980) have hypothesized, on the basis of line shifts which they interpreted as mass transfer between the stars of the binary, that large flaring episodes occur when the magnetic flux tubes of the two stars interact. In AR Lac, the large loops extend some 60% of the separation between the two stars, although not necessarily always in the

right direction to interact. It is easy to conceive that these loops may increase in length, or the loops of the G star may also grow, in order to span the gap and, perhaps, produce a large flaring episode.

Radio flares could also occur when emerging loops rising from the photosphere interact with established loops. Given the loop parameters computed above, detectable radio emission from flares due to such loop interactions will only occur at large distances from the surface, when the plasma density is low enough that the emission occurs above the plasma frequency. At lower altitudes, gyroresonance absorption or other opacity mechanisms may inhibit the escape of radio photons. The flares which occur in small loops, close to the photosphere, may be seen as X-ray, but not radio, flares, as was the case for the small X-ray flare detected during these observations.

Since the estimated number of small loops on each star is of order 10^6, little intrinsic variability outside of flaring might be expected. Because of the association of solar loops with sunspots, one may use these estimates of N as crude estimates of the number of spots on the stars in AR Lac. If 10^6 spots completely cover the star in bands between 10° and 40° latitude, then the average spot radius on the G star would be 10^8 cm (which corresponds to a typical small sunspot of 5″ diameter). More realistically, there is likely to be more than one loop per spot since solar loops are nested, and the spots are unlikely to completely cover the stellar surface, which will lead to small changes in the mean spot radius. If one attributes the bulk of the light diminution by the photometric wave to spots on the G star, then some 24% of the stellar photosphere is covered with umbra, which is consistent with the spot numbers and areas.

c) *On the Photometric Wave*

Hall, Richardson, and Chambliss (1976) showed that, at least for the past 20 years, the migration rate of the photometric wave has been constant with a period of ~ 10–15 yr. Extrapolation of this curve to 1980.5 puts wave maximum at approximately phase 0.25. This is the phase at which the X-ray flux would be expected to be greatest, since we are facing the spotted hemisphere of the star. In fact, the total X-ray flux from the system is not highest here, and no evidence for an X-ray "wave" is seen. The resolution of this conundrum may lie in the existence of two active stars in this system.

Given the continuity of the migration rate over the past century, it is likely that the dominant contribution to the photometric wave comes from one of the two stars. We have reexamined the phases of minima tabulated by Hall, Richardson, and Chambliss (1976) and find that, contrary to their conclusion that the migration period increased by a factor of 4 near 1960, the data equally well support the hypothesis that the migration rate has been constant since 1926, with a period of 12.5 ± 0.3 yr. In arriving at this result we have neglected the measurement of Ischenko (1963), which is an average of 18 years worth of observations, and we include two new measurements in 1978 and 1979 by Kurutac *et al.* (1981). The predicted phase of wave minimum in 1980.45 is 0.14 ± 0.23.

We support Kron (1947) in attributing the bulk of the optical activity to the G star. Even if both stars are equally active (same surface area covered by spots), a larger wave would be visible on the G star because of the greater luminosity contrast between the spots and the photosphere. If the spotted photospheric hemisphere is on the G star, then the brighter coronal hemisphere and the region with the bright plage activity are located above the darker optical hemisphere, as expected from solar analogy. The lack of an observed X-ray wave can be attributed to the opposite asymmetries of the coronae. The leading edge of each star is the brightest in X-rays, so that the observed flux at all phases, outside of the eclipses, is roughly constant. Some of the observed variation in optical wave amplitude may be similarly attributable to beating between the waves of each component.

d) *AR Lacertae and the Rotation-Activity Relation*

Because the eclipses allow the coronal fluxes from each star to be resolved, one can examine how each star falls in the context of the coronal rotation-activity relation. Figure 10 shows the X-ray data on the RS CVn systems and other rapidly rotating systems (both binary and single). The data are taken primarily from Walter and Bowyer (1981), Walter (1982), and Walter (1981*b*). We plot $\log L_x/L_{\rm bol}$ as a function of the stellar rotation period P. The best fix $L_x/L_{\rm bol}$ versus angular velocity ($=1/P$) relations for both the G and K stars are drawn as solid lines.

Using the linear relation between $L_x/L_{\rm bol}$ and Ω for rapidly rotating G dwarfs ($P < 11^d$) and giants (Walter 1982), it can be seen that the G component of AR Lac appears to exhibit a normal level of activity. However, the K component is underluminous relative to the mean of the K stars (Walter and Bowyer 1981) in X-rays by about a factor of 4 (Z Her and ζ And are similarly underluminous for their rotation periods). This component may be underactive because it is between stellar activity cycles (as is hypothesized for the active component of Z Her; S. Shore 1979, private communication). Given the dominance of the wave on the G star for the past 50 years, the K star may be undergoing a lengthy spell of low activity (a stellar Maunder minimum?).

It appears that the G2 IV star is a normal, active, rapidly rotating star. It also appears that the K star is less active than the mean for its spectral type, but not

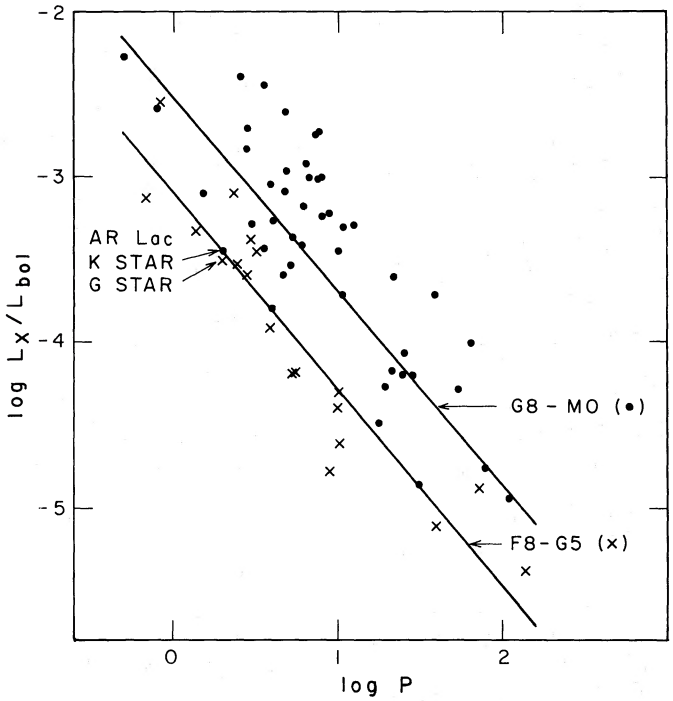

FIG. 10.—AR Lac and the rotation activity relation. The ratios of the X-ray to bolometric flux for RS CVn and other active G and K stars are plotted against their rotation periods in days. F8–G5 stars define the lower relation; G8–M0 stars define the upper relation (Walter and Bowyer 1981; Walter 1981*a*, *b*, 1982). The G component of AR Lac lies on the linear relation for active G dwarfs and giants, while the K component lies below the K star relation and appears relatively inactive, like Z Her, for its rotation period.

inordinately so. We would predict that the long term mean coronal X-ray luminosity of AR Lac should be about a factor of 3 greater than has been observed over the last 3 years.

We note that this may be a good system on which to test theories of stellar coronae. The stars are of the same age and mass, and they rotate with identical angular velocities. The chief difference is that the K star is more evolved (perhaps because of a few percent larger mass), and hence has a deeper convective zone than the G star. Extensive observations of this system will be needed to average out the intrinsic variability and clarify the spatial structures of the stellar atmospheres. Knowledge of the mean coronal and chromospheric properties of two stars which differ only in evolutionary state may constrain theories of stellar activity and dynamo action which predict scaling with macroscopic stellar parameters.

V. SUMMARY

We have obtained X-ray, radio, and ultraviolet observations of AR Lacertae over one orbital cycle. The X-ray light curve shows a deep primary minimum and a broad, shallow secondary minimum. The quiescent corona of the G2 IV component is small and asymmetric. This corona extends some 0.02 stellar radii above the photosphere; the leading, spotted hemisphere is brighter in X-rays than the trailing hemisphere. The K0 IV component has two coronal components. The extended, presumably hotter component extends to one stellar radius above the photosphere and exhibits a brighter leading hemisphere. There is an inner coronal component which is small relative to the stellar radius, but the lack of coverage past mid-eclipse severely limits our ability to deduce the nature of this component. The UV observations also imply a nonuniform surface distribution of plage regions.

The small components have physical parameters remarkably similar to an extremely active Sun covered with small flares. The extended component of the K star corona appears to consist of a small number of large loops. Such loops may well be capable of interacting with loops on the other star, as hypothesized by Simon, Linsky, and Schiffer (1980) as the cause of the large flares on RS CVn systems.

Although 60% of the coronal and chromospheric flux arises on the K star, the G star appears to be the more active star in this system. Relative to the mean of the RS CVn systems, the K star is slightly underluminous in X-rays. Contrary to the findings of Hall, Richardson, and Chambliss (1976), we find that the migration rate of the photometric wave has been constant since 1926,

which indicates that the wave likely arises predominantly on one component, the G star.

As these data show, eclipse observations can be very useful in revealing structural details of stellar atmospheres. One important lesson to be drawn from these data are that coronae and chromospheres are both highly structured and dynamic: proper analysis requires full phase coverage at many frequencies through eclipse, from well before first contact to well past fourth contact, as well as coverage at quadrature. Repeated coverage over a few orbital cycles is necessary for disentangling temporal variability from geometric eclipses. The data reported here hint at the promise of this technique for understanding stellar activity. Because of operating limitations on most types of proposed X-ray telescopes, it may be very difficult to obtain the necessary time coverage to perform this type of observation properly. The next big step in the understanding of stellar coronae, after *Einstein*, may have to await a dedicated stellar coronal X-ray observatory with moderate-to high-resolution, time-resolved spectroscopic capabilities. In the meantime, high spectral and temporal resolution of eclipsing late-type stars in the visible and UV, as will be possible with the Space Telescope High Resolution Spectrograph, hold out promise for beginning the process of understanding the structural morphology of stars other than the Sun.

We acknowledge useful discussions on stellar atmospheres with J. L. Linsky. We thank Martin Elvis and the others at CFA who saw to it that the *Einstein* observations were carried out at the proper times. We are deeply indebted to Paul A. Feldman for obtaining the simultaneous radio observations at the Algonquin Radio Observatory. Jules Halpern provided assistance with the MPC data processing and analysis. This work was financed by grants NGL-06-003-057 and NAG-8400 through the University of Colorado, NAG-8347 at NMIMT, and NAG5-69 at UCB.

REFERENCES

Agrawal, P., Riegler, G., and White, N. 1981, *M.N.R.A.S.*, **196**, 73P.
Barnes, T. G., and Evans, D. S. 1976, *M.N.R.A.S.*, **174**, 489.
Batten, A. H., Fletcher, J. M., and Mann, A. J. 1978, *Pub. Dom. Ap. Obs.*, **15**, 121.
Boggess, A., *et al.*, 1978, *Nature*, **275**, 372.
Brown, R., Broderick, J., and Neff, S. 1979, *Bull. AAS*, **11**, 630.
Chambliss, C. R. 1976, *Pub. A.S.P.*, **88**, 762.
Doschek, G. A., Feldman, U., Bhatia, A. K., and Mason, H. E. 1978*a*, *Ap. J.*, **226**, 1129.
Doschek, G. A., Feldman, U., Mariska, J. T.., and Linsky, J. L. 1978*b*, *Ap. J.* (*Letters*), **226**, L35.
Feldman, P. A., *et al.* 1978, *A.J.*, **83**, 1471.
Feldman, P. A., and Kwok, S. 1979, *J.R.A.S. Canada*, **73**, 271.
Giacconi, R. *et al.* 1979, *Ap. J.*, **230**, 540.
Giampapa, M. S., *et al.* 1982, *Ap. J.* (*Letters*), **252**, L39.
Gibson, D. M., and Hjellming, R. 1974, *Pub. A.S.P.*, **85**, 652.
Hall, D. S. 1972, *Pub. A.S.P.*, **84**, 323.
_____. 1976, in *IAU Colloquium 29, Multiple Periodic Variable Stars*, ed. W. S. Fitch (Dordrecht: Reidel).
Hall, D. S., and Kreiner, J. M. 1980, *Acta Astr.*, **30**, 387.
Hall, D. S., Richardson, T. R., and Chambliss, C. R. 1976, *A.J.*, **81**, 138.
Hjellming, R., and Blankenship, L. 1973, *Nature Phys. Sci.*, **243**, 81.
Ischenko, I. M. 1963, *Trudy Tashkent Astr. Obs.*, **9**, 25.
Joy, A. H., and Wilson, R. E. 1949, *Ap. J.*, **109**, 231.
Kane, S. R., Anderson, K. A., Evans, W. D., Klebesadel, R. W., and Laros, J. 1979, *Ap. J.* (*Letters*), **233**, L151.
Kron, G. E. 1947, *Pub. A.S.P.*, **59**, 261.
Kurutac, M. *et al.* 1981, *Ap. Space Sci.*, **77**, 325.
Lacy, C. H. 1979, *Ap. J.*, **228**, 817.
Newell, R. T., Gibson, D. M., Becker, R., and Holt, S. S. 1979, *Proc. Southwest Regional Conference for Astronomy and Astrophysics*, **5**, 1.
Owen, F., and Spangler, S. 1977, *Ap. J.* (*Letters*), **217**, L41.
Popper, D. M., and Ulrich, R. K. 1977, *Ap. J.* (*Letters*), **212**, L131.
Raymond, J., and Smith, B. 1978, *Ap. J. Suppl.*, **35**, 419.
Rosner, R., Tucker, W. H., and Vaiana, G. S. 1978, *Ap. J.*, **220**, 643.
Sanford, R. F. 1951, *Ap. J.*, **113**, 299.
Simon, T., and Linsky, J. L. 1980, *Ap. J.*, **241**, 759.
Simon, T., Linsky, J. L., and Schiffer, F. H., III. 1980, *Ap. J.*, **239**, 911.
Srivastava, R. K. 1980, *Ap. Space Sci.*, **78**, 123.
Swank, J. H. and White, N. E. 1980, in *Cool Stars, Stellar Systems, and the Sun*, ed. A. Dupree (Cambridge: Smithsonian Astrophysical Observatory).
Swank, J. H., White, N. E., Holt, S. S., and Becker, R. H. 1981, *Ap. J.*, **246**, 208.
Vaiana, G. S. and Rosner, R. 1978, *Ann. Rev. Astr. Ap.*, **16**, 393.
Walter, F. M. 1981*a*, *Ap. J.*, **245**, 677.
_____. 1981*b*, Ph.D. thesis, University of California, Berkeley.
_____. 1982, *Ap. J.*, **253**, 745.
Walter, F., and Bowyer, S. 1981, *Ap. J*, **245**, 671.
Walter, F., Cash, W., Charles, P., and Bowyer, S. 1980, *Ap. J.*, **236**, 212.
Walter, F., Charles, P., and Bowyer, S. 1978, *Ap. J.* (*Letters*), **225**, L119.
White, N. E., Sanford, P. W., and Weiler, E. J. 1978, *Nature*, **274**, 569.
Weiler, E. J., *et al.* 1978, *Ap. J.*, **225**, 919.

GIBOR S. BASRI: Space Sciences Laboratory, University of California, Berkeley, CA 94720

DAVID M. GIBSON: Department of Physics, New Mexico Institute of Mining and Technology, Socorro, NM 87801

FREDERICK M. WALTER: Joint Institute for Laboratory Astrophysics, University of Colorado, Boulder, CO 80309